Polymer Polydispersity Analysis by Thermal Diffusion Forced Rayleigh Scattering

P. Rossmanith† and W. Köhler*

Max-Planck-Institut für Polymerforschung, Postfach 3148, D-55021 Mainz, Germany

Received October 31, 1995; Revised Manuscript Received January 17, 1996[⊗]

ABSTRACT: Polydispersity effects in thermal diffusion forced Rayleigh scattering (TDFRS) on dilute polymer solutions are investigated both theoretically and experimentally and are compared to photon correlation spectroscopy (PCS). Contrary to PCS the statistical weights of the individual molar masses in the TDFRS signal can be changed by variation of the excitation pattern. With short excitation pulses the statistical weights are proportional to the concentration and independent of molar mass. The thermal diffusion coefficient D_T, the weight average Soret and diffusion coefficient, $\langle S_T \rangle_c$ and $\langle D \rangle_c$, and $\langle D \rangle_{c/D}$, from which the weight average hydrodynamic radius $\langle R_h \rangle_c$ is derived, are directly obtained from the experiment. From a deconvolution of the multiexponential decay function the molar mass distribution can be determined. Experiments are reported for solutions of polystyrene in toluene and ethyl acetate and for polystyrene microgels in toluene. The thermal diffusion coefficient of polystyrene in ethyl acetate is obtained as $D_T = 1.31 \times 10^{-7}$ cm^2 (s K)$^{-1}$ ($T = 24$ °C).

Introduction

The Ludwig−Soret effect, also termed thermal diffusion, describes the coupling between a temperature gradient and a resulting mass flux in multicomponent systems. On a phenomenological level experiments are described in terms of diffusion equations with the transport coefficients, which are the thermal diffusivity D_{th}, the mutual diffusion coefficient D, and the thermal diffusion coefficient D_T, as parameters. Of particular interest is the molar mass dependence of the Soret coefficient of $S_T = D_T/D$, which, though not very well understood on a microscopic level,[1,2] can be utilized for polymer fractionation in thermal field flow fractionation (TFFF).[3−5]

Thermal diffusion forced Rayleigh scattering (TDFRS) provides a sensitive optical tool for the study of thermal and mutual diffusion.[6−9] A holographic temperature grating is written into the solution and, due to the Ludwig−Soret effect, gives rise to a concentration grating. The time evolution of both gratings is monitored by Bragg diffraction of a readout beam. This technique provides certain advantages when compared to more traditional methods, such as thermal diffusion cells,[2,10] thermogravitational columns,[11] or TFFF. The microscopic diffusion lengths result in short diffusion times (milliseconds to seconds), which make the experiment insensitive to perturbations. The very subtle temperature modulations of the order of several microkelvin ensure that the system stays close to thermal equilibrium.

The time evolution of the concentration grating is governed by the mutual diffusion coefficient and the corresponding heterodyne diffraction efficiency reveals some similarities to the electric field autocorrelation function in photon correlation spectroscopy (PCS). For dilute monodisperse samples, which are characterized by a single diffusion coefficient, the information content of both normalized decay functions is almost identical and the diffusion coefficient can be translated into a hydrodynamic particle radius by means of the Stokes−Einstein relation. With a proper scaling relation $D = a'M^{-b}$, the molar mass can be determined.

For polydisperse samples the situation is different. The decay function is no longer single exponential but a linear superposition of the contributions from the individual components. For PCS the statistical weights are fixed and proportional to cM, c being the concentration. The excitation of TDFRS, on the other hand, lies in the hands of the experimentalist. The variation of the excitation pattern allows the variation of the relative statistical weights of the individual signal contributions.[12]

In this paper the equations for a description of TDFRS experiments on polydisperse samples will be derived and applied to various polystyrene solutions with particular emphasis on the similarities and differences between PCS and TDFRS.

Theory

Monodisperse Samples. Before turning to polydispersity effects, the equations for monodisperse systems will briefly be summarized.[6,8,13]

A holographic optical interference grating with an intensity distribution

$$I(x,t) = I_0 + I_q(t)e^{iqx} \tag{1}$$

is written into the sample with the x-axis defined by the grating vector $q = 4\pi\lambda^{-1}\sin(\theta/2)$. θ is the angle of intersection between the two writing beams. The constant average intensity I_0 accounts for polarization switching,[9] which ensures a constant spatially averaged thermal load on the sample. The spatial and temporal evolution of the temperature distribution is obtained from the heat equation with the absorbed energy as the source term:

$$\frac{\partial T(x,t)}{\partial t} = D_{th}\frac{\partial^2}{\partial x^2}T(x,t) + s(x,t) \tag{2}$$

$$s(x,t) = \frac{\alpha}{\rho c_p}I(x,t) = s_0 + s_q(t)e^{iqx} \tag{3}$$

D_{th} is the thermal diffusivity, α the optical absorption

* To whom correspondence should be addressed.
† Present address: Kunststofflaboratorium, BASF-Aktiengesellschaft, D-67056 Ludwigshafen am Rhein, Germany.
⊗ Abstract published in *Advance ACS Abstracts,* March 1, 1996.

0024-9297/96/2229-3203$12.00/0 © 1996 American Chemical Society

coefficient, ρ the density, and c_p the specific heat of the solution at constant pressure. Equation 2 is solved by

$$T(x,t) = T_0 + T_q(t)\mathrm{e}^{iqx} \tag{4}$$

$$T_q(t) = \int_{-\infty}^{t} \mathrm{d}t'\, s_q(t')\mathrm{e}^{-(t-t')/\tau_{th}} \tag{5}$$

where T_0 is the average sample temperature and $\tau_{\mathrm{th}} = (D_{\mathrm{th}}q^2)^{-1}$.

When $T(x,t)$ is known the evolution of the concentration grating driven by the Ludwig−Soret effect is found from an extension of Fick's second law of diffusion:[14]

$$\frac{\partial c(x,t)}{\partial t} = D\frac{\partial^2}{\partial x^2}c(x,t) + D_T c(x,t)[1 - c(x,t)]\frac{\partial^2}{\partial x^2}T(x,t) \tag{6}$$

$D = (\tau q^2)^{-1}$ and D_T are the ordinary and the thermal diffusion coefficient, respectively. c is the concentration in weight fractions. With the approximation $c(x,t)[1 - c(x,t)] \approx c_0(1 - c_0)$,[8] eq 6 is solved by

$$c(x,t) = c_0 + c_q(t)\mathrm{e}^{iqx} \tag{7}$$

$$c_q(t) = -q^2 D_T c_0(1 - c_0)\int_{-\infty}^{t} \mathrm{d}t'\, T_q(t')\mathrm{e}^{-(t-t')/\tau} \tag{8}$$

The resulting phase grating with contributions from both temperature and concentration is read by Bragg diffraction of a readout beam at a wavelength where the sample is fully transparent. After normalization to the steady state amplitude of the thermal signal, δT, the heterodyne diffraction efficiency, which is proportional to the refractive index grating modulation depth, is obtained:

$$\zeta_{\mathrm{het}}(t) = \delta T^{-1} \int_{-\infty}^{t} \mathrm{d}t'\, G(t - t')T_q(t') \tag{9}$$

Here, the linear response function $G(t)$ is defined as

$$G(t) = \begin{cases} \delta(t) - \left(\frac{\partial n}{\partial c}\right)_{p,T}\left(\frac{\partial n}{\partial T}\right)_{p,c}^{-1} q^2 D_T c_0(1 - c_0)\mathrm{e}^{-t/\tau} & t \geq 0 \\ 0 & t < 0 \end{cases} \tag{10}$$

$\delta T = \tau_{\mathrm{th}} s_0$ holds for a grating with 100% modulation depth.

Heterogeneous Samples. A polydisperse or otherwise heterogeneous sample can no longer be characterized by a single relaxation process. In the limit of infinite dilution, where $c_0(1 - c_0) \approx c_0 = \sum_k c_{0,k}$, eq 6 can be solved independently for every component k:

$$c_k(x,t) = c_{0,k} + c_{q,k}(t)\mathrm{e}^{iqx} \tag{11}$$

$$c_{q,k}(t) = -q^2 D_{T,k} c_{0,k}\int_{-\infty}^{t} \mathrm{d}t'\, T_q(t')\mathrm{e}^{-(t-t')/\tau_k} \tag{12}$$

The normalized heterodyne diffraction efficiency is still obtained from eq 9 after rewriting the response function $G(t)$ as a linear superposition of the individual contributions:

$$G(t) = \sum_k G_k(t) = \delta(t) + \sum_k a_k e^{-t/\tau_k} \tag{13}$$

$$a_k = -q^2\left(\frac{\partial n}{\partial T}\right)_{p,c}^{-1}\left(\frac{\partial n}{\partial c_k}\right)_{p,T,c_{l\neq k}} D_{T,k}c_{0,k} \tag{14}$$

The quantities that can potentially be different for the individual components are labeled with the summation index k in eqs 13 and 14. They comprise the diffusion time constant $\tau_k = (D_k q^2)^{-1}$, the thermal diffusion coefficient $D_{T,k}$, the concentration of the kth component $c_{0,k}$, and the refractive index derivative $(\partial n/\partial c_k)_{p,T,c_{l\neq k}}$. The subscripts at the refractive index derivative indicate that for its measurement the pressure, p, the temperature, T, and the concentrations of all components $l \neq k$, c_l, are kept constant.

In dilute polymer solutions D_{th} is typically 3−4 orders of magnitude larger than D and the retardation in eq 5 can safely be neglected. Hence, the temperature grating follows the optical intensity grating instantaneously with an amplitude

$$T_q(t) = \tau_{\mathrm{th}} s_q(t) = \tau_{\mathrm{th}}\frac{\alpha}{\rho c_p} I_q(t) \tag{15}$$

While this approximation is not strictly necessary for the following discussion, it simplifies the resulting equations considerably, since the optical interference grating can be taken directly as the driving source for the concentration grating,[8] and eqs 9, 13, 14, and 15 will be used as the starting point for the treatment of polydispersity effects in TDFRS. In the next section the response of the sample will be calculated for some excitation patterns of practical interest.

Time Domain Experiments. Usually, experiments are performed in the time domain and the diffracted signal is measured during and after an excitation pulse of finite duration τ_p. Depending on the length of the pulse with respect to the relaxation times τ_k, different statistical weights will be obtained for the individual components.

From eqs 9 and 13 the heterodyne diffraction efficiency for a steplike excitation starting at $t = 0$,

$$T_q(t) = \delta T h(t) \tag{16}$$

is obtained as[8]

$$\zeta_{\mathrm{het}}(t) = h(t)[1 + \sum_k a_k\tau_k(1 - \mathrm{e}^{-t/\tau_k})] \tag{17}$$

$h(t)$ is the Heaviside step function.

Similarly, the response to an excitation pulse of length τ_p,

$$T_q(t) = \delta T(h(t + \tau_p) - h(t)) \tag{18}$$

which lasts from $t = -\tau_p$ to $t = 0$, is derived. After the temperature grating is switched off at $t = 0$, the temperature signal disappears instantaneously and the concentration signal decays as

$$\zeta_{\mathrm{het}}(t) = \sum_k a_k\tau_k(1 - \mathrm{e}^{-\tau_p/\tau_k})\mathrm{e}^{-t/\tau_k} \tag{19}$$

resulting in a multiexponential decay function with a

statistical weight

$$a_k\tau_k(1 - e^{-\tau_p/\tau_k}) \tag{20}$$

for the kth mode, which depends on the duration τ_p of the excitation pulse.

Of special interest are very short excitations with $\tau_p \ll \tau_k$ (δ pulses) and very long excitations with $\tau_p \gg \tau_k$, where the plateau value of the diffraction efficiency is reached for all modes. In both cases the statistical weights of the decay function after the grating is switched off takes a particularly simple form:

$$\zeta_{het}(t) = \begin{cases} \sum_k a_k\tau_p e^{-t/\tau_k} & \tau_p \ll \tau_k \\ \sum_k a_k\tau_k e^{-t/\tau_k} & \tau_p \gg \tau_k \end{cases} \tag{21}$$

Frequency Domain Experiments. Experiments may also be performed in the frequency domain[15] with a sinusoidal amplitude modulation of the holographic interference grating, suitable for lock-in detection. No such experiments will be reported in this paper; however the necessary formulas are given below for completeness:

$$T_q(t) = \delta T e^{iwt} \tag{22}$$

$$\zeta_{het}(t) = \chi(\omega)e^{iwt} \tag{23}$$

The susceptibility $\chi(\omega)$, which is directly measured as the complex amplitude in a frequency domain experiment, is the Fourier transform of the linear response function $G(t)$:

$$\chi(\omega) \equiv 2\pi\tilde{G}(\omega) = \int_{-\infty}^{\infty} dt\, e^{iwt}G(t) = 1 + \sum_k a_k \frac{\tau_k}{1 + i\omega\tau_k} \tag{24}$$

After the convolution theorem is employed, eq 9 takes the simple product form in the frequency domain:

$$\tilde{\zeta}_{het}(\omega) = \delta T^{-1}\tilde{T}(\omega)\chi(\omega) \tag{25}$$

$\tilde{\zeta}_{het}(\omega)$ and $\tilde{T}(\omega)$ are defined in analogy to $\tilde{G}(\omega)$ in eq 24.

Averages and Distribution Functions. In this section the various averages that can be derived from TDFRS measurements on polydisperse samples will be summarized. For this purpose two more approximations will be made.

First, for homopolymers, the concentration derivative of the refractive index is approximately constant over a broad molar mass range, where end group effects can be neglected. Furthermore, the molar mass independence of D_T is well established for a wide variety of polymers and seems to be a universal property.[1,2,5,8] In this case eq 14 simplifies to

$$a_k = -q^2\left(\frac{\partial n}{\partial T}\right)_{p,c}^{-1}\left(\frac{\partial n}{\partial c}\right)_{p,T} D_T c_{0,k} \tag{26}$$

Statistic copolymers are an example where eq 14 generally cannot be simplified, since there is a distribution of the chemical composition even for a given degree of polymerization, and hence a distribution of $(\partial n/\partial c_k)_{p,T,c_{l\neq k}}$, $D_{T,k}$, and τ_k.

Initial Rise. After the temperature grating is switched on, the initial linear rise of the concentration grating according to eq 17 leads to

$$\zeta_{het}(t > 0) \approx 1 + \sum_k a_k t = 1 - q^2\left(\frac{\partial n}{\partial T}\right)_{p,c}^{-1}\left(\frac{\partial n}{\partial c}\right)_{p,T} c_0\langle D_T\rangle_c t \tag{27}$$

c_0 is the total polymer concentration and $\langle D_T\rangle_c \approx D_T$ the weight average thermal diffusion coefficient. The subscript indicates the statistical weight used for averaging:

$$\langle D_T\rangle_c = \frac{\sum_k c_{0,k}D_{T,k}}{c_0} \qquad c_0 = \sum_k c_{0,k} \tag{28}$$

Hence, the thermal diffusion coefficient, or its weight average in the case of a molar mass dependence, is obtained from the initial rise of ζ_{het}, irrespective of sample polydispersity.

Plateau Value. After an excitation time $t \gg \tau_k$ the plateau value is reached (eq 17) with an amplitude of

$$\zeta_{het}(t \gg \tau_k) = 1 + \sum_k a_k\tau_k = 1 - \left(\frac{\partial n}{\partial T}\right)_{p,c}^{-1}\left(\frac{\partial n}{\partial c}\right)_{p,T} c_0\langle S_T\rangle_c \tag{29}$$

$\langle S_T\rangle_c = \langle D_T/D\rangle_c$ is the weight average Soret coefficient. The same amplitude is measured in a frequency domain experiment (eq 24) for $\chi(\omega \to 0)$.

Decay Functions. As already pointed out, the concentration signal decays multiexponentially after the temperature grating is turned off, the statistical weights for the individual modes depending on the duration of the excitation pulse (eqs 20 and 21). Several ways of dealing with a multiexponential decay can be found in the literature.

If only the average, the width, and possibly the skewness of a not too broad rate distribution function are of interest, a cumulant expansion is appropriate:[16,17]

$$\frac{\zeta_{het}(t)}{\zeta_{het}(0)} = e^{-\langle\Gamma\rangle t + (1/2)\mu_2 t^2 - (1/6)\mu_3 t^3 + \ldots} \tag{30}$$

$\langle\Gamma\rangle = \langle\tau^{-1}\rangle$ is the average decay rate and $\mu_2 = \langle(\Gamma - \langle\Gamma\rangle)^2\rangle$ is the second and $\mu_3 = \langle(\Gamma - \langle\Gamma\rangle)^3\rangle$ the third cumulant, which determine the width and the skewness of the rate distribution. From eq 21, together with $D = \Gamma q^{-2}$, the average diffusion coefficients in the long and short exposure limit follow immediately:

$$q^{-2}\langle\Gamma\rangle = \begin{cases} \langle D\rangle_c & \tau_p \ll \tau_k \\ \langle D\rangle_{c/D} & \tau_p \gg \tau_k \end{cases} \tag{31}$$

The same statistical weights apply for μ_2. Thus, in the short exposure limit, TDFRS gives access to the weight average diffusion coefficient, in contrast to PCS, which measures the z-average $\langle D\rangle_{cM}$, M being the molar mass.

Other algorithms, like CONTIN,[18] allow the numerical computation of the entire rate distribution $P(\Gamma)$ from the experimentally observed decay function. A detailed analysis of various inversion techniques for PCS experiments and their application to polymer polydispersity

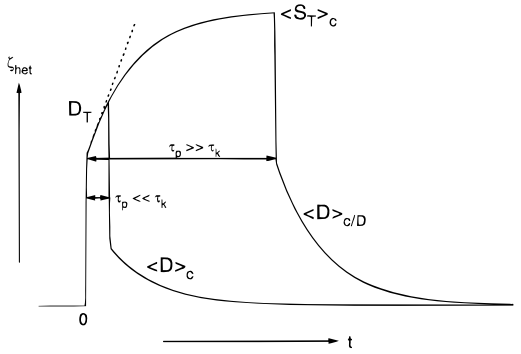

Figure 1. Average transport coefficients that can be obtained from a pulsed TDFRS experiment with excitation length τ_p.

analysis can be found in refs 17, 19, and 20. As far as the rate distribution is concerned, similar arguments apply to TDFRS. The situation is different, however, for the molar mass distribution, as will be discussed in the next section.

Figure 1 summarizes the averages that can be obtained from the various experiments. Besides from the initial slope (eq 27), a molar mass independent D_T can also be calculated from the long exposure limit Soret (eq 29) and diffusion (eq 31) coefficients:

$$\langle S_T\rangle_c\langle D\rangle_{c/D} = D_T\langle D^{-1}\rangle_c\langle D^{-1}\rangle_c^{-1} = D_T \tag{32}$$

Weight Average Hydrodynamic Radius. Of special interest is the possibility to measure the true weight average hydrodynamic radius, $\langle R_h\rangle_c$, of polymer molecules or colloidal particles, contrary to PCS, which yields the inverse *z*-average $\langle R_h^{-1}\rangle_{cM}^{-1}$. This can be seen as follows.

R_h and D in the limit of infinite dilution are related by the Stokes−Einstein relation

$$D = \frac{kT}{6\pi\eta_0 R_h} \tag{33}$$

η_0 is the solvent viscosity. In the long exposure limit, $\tau_p \gg \tau_k$, $\langle D\rangle_{c/D}$ is obtained from TDFRS (eq 31), and by employing eq 33,

$$\frac{6\pi\eta_0}{kT}\langle D\rangle_{c/D} = \langle R_h^{-1}\rangle_{c/D} = \langle R_h^{-1}\rangle_{cR_h} = \frac{\sum_k c_{0,k}R_{h,k}R_{h,k}^{-1}}{\sum_k c_{0,k}R_{h,k}} = \langle R_h\rangle_c^{-1} \tag{34}$$

Molar Mass Distribution. A scaling relation

$$\Gamma = q^2D = aM^{-b} \tag{35}$$

relates the diffusion coefficient of a polymer at infinite dilution, and hence the decay rate Γ, to its molar mass.[20] The exponent b is characteristic for the morphology of the particle. Typical values are $^1/_3$ for a solid sphere, 0.5−0.6 for a random coil, depending on the solvent quality, and 1 for a rigid rod.

In the following, molar mass distributions and averages as obtained from TDFRS will be compared to PCS results. Both techniques measure multiexponential decay (correlation) functions, however with different statistical weights for the individual molar masses.

Strictly speaking, D is the diffusion coefficient in the limit $q \to 0$. PCS measurements are usually performed for $qR_g \leq 1$, R_g being the radius of gyration, where internal modes of the polymer molecule cannot be neglected. The scattering angles for TDFRS are of the order of 1°, hence $qR_g \ll 1$, where the extrapolation $q \to 0$ can safely be omitted. While these small scattering angles are ideal for a heterodyne TDFRS experiment, they are very difficult to realize with PCS.[20]

With eqs 21, 26, and 35 the normalized heterodyne decay function, or the electric field autocorrelation function in the case of PCS, can be written in a general form as

$$\frac{\zeta_{het}(t)}{\zeta_{het}(0)} = \sum_k p_k e^{-t/\tau_k} \qquad p_k = \frac{c_{0,k}M_k^\alpha}{\sum_k c_{0,k}M_k^\alpha} \tag{36}$$

The exponent α is characteristic for the experiment:

$$\alpha = \begin{cases} 0 & \text{TDFRS } (\tau_p \ll \tau_k) \\ b & \text{TDFRS } (\tau_p \gg \tau_k) \\ 1 & \text{PCS} \end{cases} \tag{37}$$

Once the rate distribution $P(\Gamma)$ is known, e.g. from CONTIN, the calculation of the molar mass distribution $c(M)$ by means of eq 35 is straightforward and best formulated using a continuous notation:

$$c(M) \propto P(\Gamma(M))M^{-\alpha}\left|\frac{d\Gamma(M)}{dM}\right| \propto P(\Gamma(M))M^{-1-b-\alpha} \tag{38}$$

In the case of arbitrary excitation length TDFRS the molar mass distribution is given by

$$c(M) \propto P(\Gamma(M))(1 - e^{-\Gamma\tau_p})^{-1}\, M^{-1-2b} \tag{39}$$

The weight and number average molar masses, M_w and M_n, can be determined directly from the rate distribution:

$$M_w \equiv \langle M\rangle_c = a^{1/b}\langle\Gamma^{(\alpha-1)/b}\rangle_{cM^\alpha}\langle\Gamma^{\alpha/b}\rangle_{cM^\alpha}^{-1} \tag{40}$$

$$M_n \equiv \langle M\rangle_{c/M} = a^{1/b}\langle\Gamma^{\alpha/b}\rangle_{cM^\alpha}\langle\Gamma^{(\alpha+1)/b}\rangle_{cM^\alpha}^{-1} \tag{41}$$

The index cM^α indicates that the unmodified rate distribution function, as obtained from the respective experiment (eq 37), is used for computation of the averages.

Similar considerations can be made when only the first moments or cumulants of the rate distribution are known, e.g. from a cumulant expansion. For this purpose the nth moment of the relaxation rate is expressed in terms of weight averages of the molar mass distribution:

$$\langle\Gamma^n\rangle_{cM^\alpha} = a^n\langle M\rangle_c^{-nb}\left[1 + \frac{1}{2}nb(nb - 2\alpha + 1)\langle\epsilon^2\rangle_c + O(\epsilon^3)\right] \tag{42}$$

In above equation only terms up to second order in $\epsilon_k = (M_k\langle M\rangle^{-1} - 1)$ have been taken into account. Within the same approximation the polydispersity can be introduced:

$$\frac{M_w}{M_n} \approx \langle\epsilon^2\rangle_c + 1 \tag{43}$$

From eq 42 it follows immediately that the width of the rate distribution is related to the polydispersity by

$$\frac{\langle \Gamma^2 \rangle_{cM^\alpha} - \langle \Gamma \rangle_{cM^\alpha}{}^2}{\langle \Gamma \rangle_{cM^\alpha}{}^2} = b^2 \left(\frac{M_w}{M_n} - 1 \right) \tag{44}$$

Interestingly, the right side of eq 44 is independent of α, and hence independent of the type of experiment performed.

As a consequence of eq 42, the diffusion coefficient measured by PCS, $\langle D \rangle_{cM}$, is always smaller than the one measured by TDFRS:

$$\frac{\langle D \rangle_{cM}}{\langle D \rangle_c} = 1 - b \left(\frac{M_w}{M_n} - 1 \right) \tag{45}$$

$$\frac{\langle D \rangle_{cM}}{\langle D \rangle_{cM^b}} = 1 - b(1-b) \left(\frac{M_w}{M_n} - 1 \right) \tag{46}$$

An equation similar to eq 46 has already been derived by Corti and co-workers in ref 21.

Experimental Section

All details of the TDFRS experiment have been described in previous publications.[6−9] The important features are heterodyne detection with active phase tracking and polarization switching of the grating. The solutions were slightly colored with quinizarin. An argon ion laser operating at 488 nm was used for writing and a helium neon laser at 632.8 nm for reading of the grating. Typical laser intensities were of the order of 50 mW cm^{-2}. The independence of the results from the intensity of the writing laser has been checked. The optical path length within the cuvette was 100 or 200 μm. Most measurements were averaged over several hours, in some cases overnight.

High-quality solvents (for chromatography) were used. The polystyrene (PS) standards were obtaind from Polymer Standards Service, Mainz, and have been cross-checked by size exclusion chromatography (SEC). The PS with the broad molar mass distribution was synthesized by radical polymerization. The PS microgels were synthesizd with a cross-link ratio of 1:20 by radical copolymerization of styrene and diisopropenylbenzene as cross-linker in an emulsion. Details about their synthesis and characterization can be found in ref 22.

The PCS measurements were made with a commercial light scattering setup (ALV, Langen), equipped with a krypton ion laser (647 nm) and an ALV 3000 digital correlator.

A standard SEC setup (Waters) and PS calibration was used for the SEC measurements.

The contrast factors $(\partial n/\partial c)_{p,T}$ and $(\partial n/\partial T)_{p,c}$ were measured with a scanning Michelson interferometer. Details of the measurement can be found in ref 23.

Results and Discussion

Narrow Distributions. In the following section diffusion coefficients measured with TDFRS and PCS will be compared. Unless stated otherwise, long exposure TDFRS ($\tau_p \gg \tau_k$) has been used. In most cases the experiments have been conducted at slightly different temperatures of typically 24 °C in case of TDFRS and 22−23 °C in case of PCS. To compare the results, a temperature correction according to eq 33 is necessary, with an Arrhenius type activation for the solvent viscosity: $\eta_0 \propto \exp(-E_a/RT)$; E_a = 8820 J mol^{-1} for toluene and E_a = 8464 J mol^{-1} for ethyl acetate.[1] The apparent hydrodynamic radius R_h is assumed as independent of temperature for the narrow temperature interval of interest.

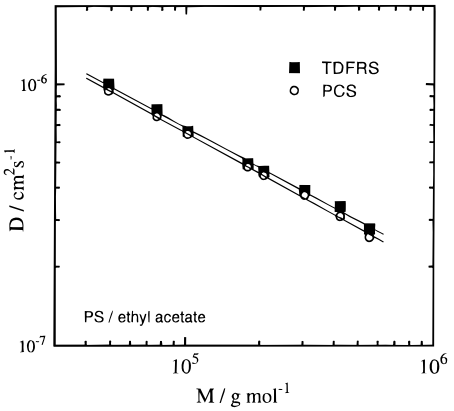

Figure 2. Average diffusion coefficients as obtained from a cumulant fit for nearly monodisperse PS standards in ethyl acetate as a function of molar mass. Concentration $c_0 = 0.006$.

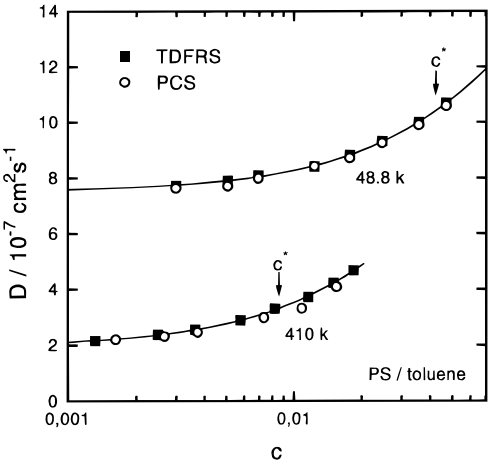

Figure 3. Average diffusion coefficients as obtained from a cumulant fit for nearly monodisperse PS standards in toluene as a function of concentration. M_w = 48.8 and 410 kg mol^{-1}.

Linear Polystyrene. The diffusion coefficients of a series of narrow PS calibration standards with molar masses between 40 and 600 kg mol^{-1}, dissolved in ethyl acetate, has been measured with TDFRS and PCS at a concentration of $c_0 = 0.005$. Due to the marginal solvent quality of ethyl acetate for PS, an extrapolation to zero concentration can usually be omitted for this system.[24] Figure 2 shows the respective diffusion coefficients as obtained from a cumulant fit to the decay functions. Similar results are obtained from a CONTIN analysis. Both data sets fall nicely onto straight lines in the double logarithmic plot, from which the scaling relation $D = a'M^{-b}$ (eq 35) is obtained with $a' = 2.76 \times 10^{-4}$ cm^2 s^{-1}, $b = 0.525$ for PCS and $a' = 2.57 \times 10^{-4}$ cm^2 s^{-1}, $b = 0.516$ for TDFRS. Within the experimental error both slopes are equal and close to 0.5, characteristic for Θ-solvents.

For two PS samples the concentration dependence of the diffusion coefficient in the dilute regime has been measured using toluene as solvent.[8] The data are plotted in Figure 3, where the respective overlap concentration $c^* = [\eta]^{-1}$ is marked with an arrow.

A good agreement between PCS and TDFRS has been found in both experiments, with PCS yielding systematically lower values. The difference of a few percent is just above the experimental resolution and in accordance with eq 46, which predicts approximately 1% difference for random coils ($b \approx 0.5$) with polydispersities of 1.03−1.05, as employed for the experiment.

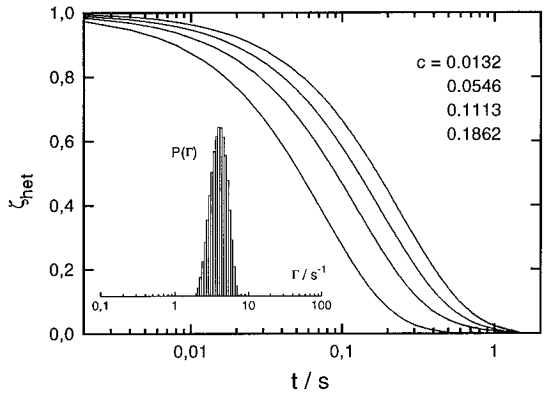

Figure 4. Normalized heterodyne decay functions for PS microgels in toluene at four different concentrations. The insert shows a CONTIN analysis of the rate distribution for the lowest concentration.

Table 1. CONTIN Analysis of PS Microgels in Toluene

c	Γ/s^{-1}	$D/10^{-7}$ cm^2 s^{-1}	$(\mu_2/\langle\Gamma\rangle^2)^{1/2}$
0.0132	4.19	2.13	0.28
0.0546	5.50	2.79	0.29
0.1113	7.74	3.93	0.25
0.1862	13.2	6.70	0.24

Microgels. PS microgels with a cross-link ratio of 1:20 have been used as model systems for compact spheres.[22] The normalized heterodyne decay functions of the concentration grating (Figure 4) have been analyzed using CONTIN for a series of four different concentrations. The rate distribution as obtained from the lowest concentration is plotted in Figure 4 as an insert.

The average diffusion coefficients, $\langle D\rangle_{cM^b}$, as obtained from the average rate, and the width of the rate distribution are summarized in Table 1.

The diffusion coefficient can be extrapolated to zero concentration by a second-order polynomial, $\langle D\rangle_{cM^b} = (2.07 + 0.062c + 0.01c^2) \times 10^{-7}$ cm^2 s^{-1}. From eq 34 the weight average hydrodynamic radius is obtained as $\langle R_h\rangle_c = 19.0$ nm. The width of the rate distribution is, within the experimental error, almost independent of concentration. Using $[\langle R_h^2\rangle_c/\langle R_h\rangle_c^2 - 1]^{1/2} = (\mu_2/\langle\Gamma\rangle^2)^{1/2} = 0.27$ and the hard sphere value $b = {}^1/_3$, the molar mass polydispersity $M_w/M_n = 1.7$ can be calculated from eq 44.

The diffusion coefficient of a similar microgel has been measured with both TDFRS and PCS, and a distribution width of $(\mu_2/\langle\Gamma\rangle^2)^{1/2} = 0.24$ was found, corresponding to $M_w/M_n = 1.52$ according to eq 44. The measured hydrodynamic radii are $\langle R_h\rangle_c = 23.7$ nm (TDFRS) and $\langle R_h^{-1}\rangle_{cM}^{-1} = 26.5$ nm (PCS). From their ratio $\langle R_h\rangle_c/\langle R_h^{-1}\rangle_{cM}^{-1} = 0.89$ the polydispersity can also be calculated according to eq 46, which yields $M_w/M_n = 1.48$, in very good agreement with the value of 1.52 determined from the width of the rate distribution.

Broad Distributions. Mixtures of PS of two different molar masses ($M_{w,1} = 48$ kg mol^{-1} and $M_{w,2} = 556$ kg mol^{-1}) have been used as model systems for polydisperse polymers. To investigate the dependence of the individual statistical weights on the exposure time, a mixture containing both molar masses at equal parts has been dissolved in ethyl acetate at a concentration of $c_0 = c_{0,1} + c_{0,2} = 0.0058$. The exposure was varied between 0.025 and 2 s at a grating vector $q = 4000$ cm^{-1}, and the normalized heterodyne signals are shown in Figure 5.

From the molar mass dependence of the relaxation rate (Figure 2) the relaxation times of the two species

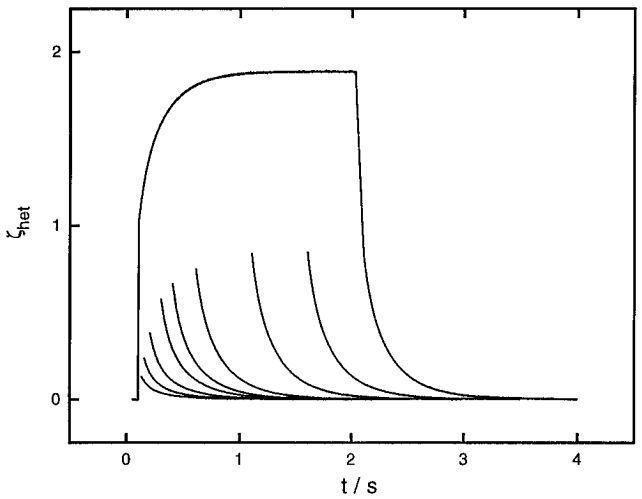

Figure 5. Decay functions for exposure times between 0.025 and 2 s for a bimodal mixture of PS in ethyl acetate. $M_{w,1} = 49$ kg mol^{-1}, $M_{w,2} = 556$ kg mol^{-1}, equal concentrations of both components.

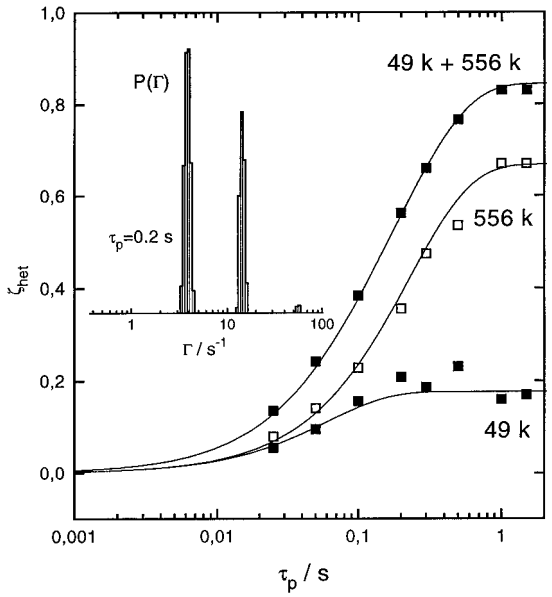

Figure 6. Amplitudes of the two modes from Figure 5 as a function of exposure time τ_p. The insert shows the rate distribution for $\tau_p = 0.2$ s.

are obtained as $\tau_1 = 0.064$ s and $\tau_2 = 0.224$ s. Hence, the exposure times τ_p cover the range from significantly shorter than the fastest to much longer than the slowest mode. CONTIN was used for the analysis of the decay curves, and bimodal rate distributions have been found for all exposure times. The rate distribution for the 0.2 s exposure is shown as an insert in Figure 6.

The main part of Figure 6 shows the amplitudes of the two relaxation modes as a function of the exposure time. The solid lines are the predictions according to eq 20, with the relaxation times τ_k taken from the scaling relation in Figure 2 and the amplitudes a_k calculated from eq 14. The measurement of the thermal diffusion coefficients will be described later.

The individual relaxation rates for the slow and the fast mode are independent of exposure time and close to the numbers calculated from the scaling relation: $\bar{\Gamma}_{49k} = 16.4$ s^{-1} as compared to 15.6 s^{-1} from eq 37, and $\bar{\Gamma}_{556k} = 4.34$ s^{-1} as compared to 4.46 s^{-1}.

Figure 7 shows a plot of various averages of the relaxation rate. The average rate, $\langle\Gamma\rangle$, decreases with

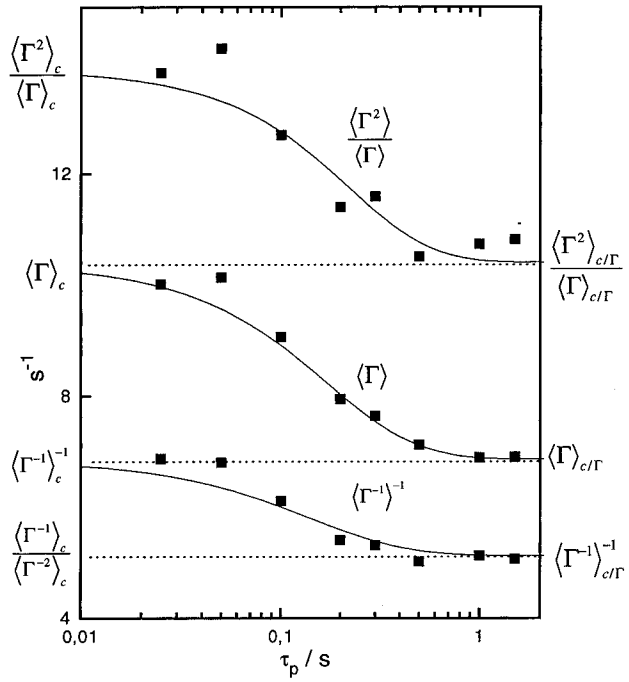

Figure 7. Various rate averages from Figure 5 as a function of exposure time τ_p. See text for details.

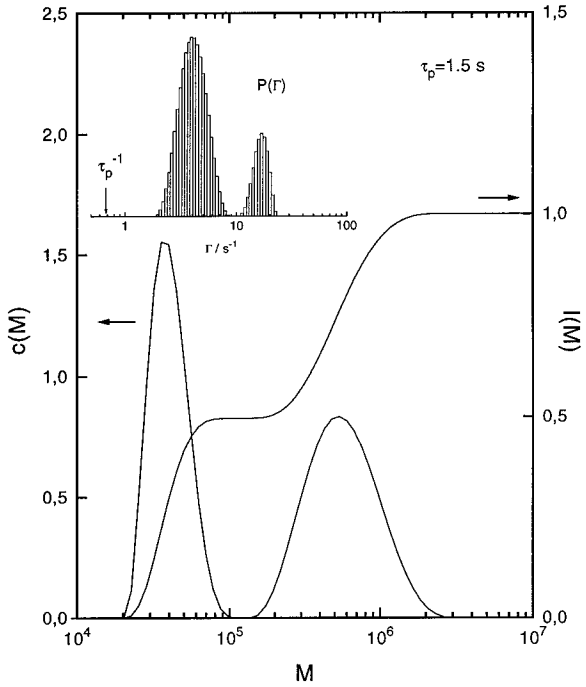

Figure 8. Differential ($c(M)$) and integral ($I(M)$) molar mass distribution calculated from the decay function in Figure 5 in the long exposure limit (τ_p = 1.5 s). The rate distribution in the insert was obtained from CONTIN.

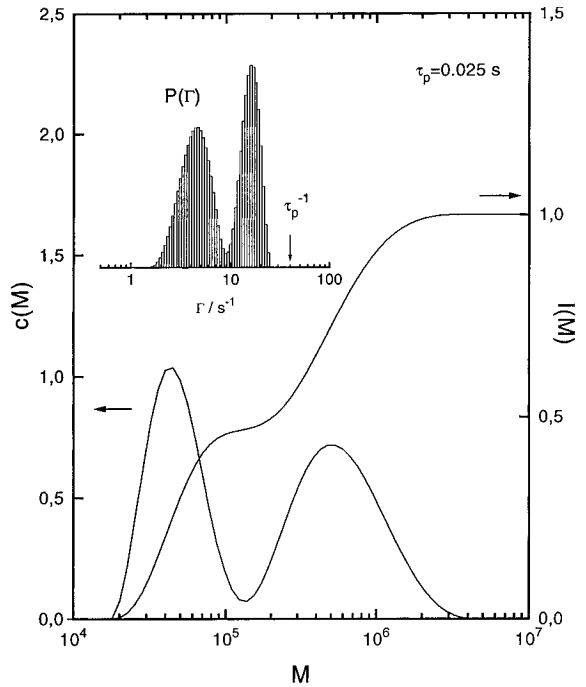

Figure 9. Same as Figure 8, however in the short exposure limit (τ_p = 0.025 s).

increasing exposure time from $\langle\Gamma\rangle_c$ to $\langle\Gamma\rangle_{c/\Gamma}$. Similarly, $\langle\Gamma^2\rangle\langle\Gamma\rangle^{-1}$ decreases from $\langle\Gamma^2\rangle_c\langle\Gamma\rangle_c^{-1}$ to $\langle\Gamma^2\rangle_{c/\Gamma}\langle\Gamma\rangle_{c/\Gamma}^{-1}$ and $\langle\Gamma^{-1}\rangle^{-1}$ from $\langle\Gamma^{-1}\rangle_c^{-1}$ to $\langle\Gamma^{-1}\rangle_{c/\Gamma}^{-1}$. The solid lines are calculated with the statistical weights according to eq 20. Especially $\langle\Gamma\rangle$ can be determined very precisely and the experimental data coincide, with the exception of the value at τ_p = 0.05 s, nearly perfectly with the theoretical curve. Note that $\langle\Gamma\rangle_c = \langle\Gamma^2\rangle_{c/\Gamma}\langle\Gamma\rangle_{c/\Gamma}^{-1}$ and $\langle\Gamma^{-1}\rangle_c\langle\Gamma^{-2}\rangle_c^{-1} = \langle\Gamma^{-1}\rangle_{c/\Gamma}^{-1}$, which is indicated by the horizontal dotted line. Hence, the second moment of the rate in the long exposure limit can be obtained from a measurement of the first moment in the short exposure limit.

Molar Mass Distribution. The molar mass distribution $c(M)$ has been computed from the rate distribution $P(\Gamma)$ according to eq 38 for the bimodal mixtures in the long and short exposure limit, corresponding to τ_p = 1.5 s and τ_p = 0.025 s, and the results are shown in Figures 8 and 9. The rate distributions as obtained from the respective decay functions (Figure 5) are plotted as inserts.

The inverse exposure times τ_p^{-1}, which are well below and above the limits of the rate distributions, are marked with arrows. Note the differences in the relative intensities of the fast and the slow mode. With the correct statistical weights according to eqs 37 and 38, nearly identical molar mass distributions are obtained. The peak maxima coincide with the molar masses of the PS standards used, and the two peak areas are almost equal, as can be seen from the plateau close to 0.5 in the integral molar mass distribution.

Contrary to the peak positions and the overall width, the width of the individual peaks in a multimodal distribution are less reproducible. This problem is frequently encountered in a CONTIN analysis and best illustrated by comparing the rate distributions in Figures 6, 8, and 9, which all belong to the same sample.

A broad PS obtained by radical polymerization has been used as a model system for a broad unimodal molar mass distribution. Again, ethyl acetate was used as solvent and the concentration was c_0 = 0.005. In order to compare the different techniques measurements have been made with short and long exposure TDFRS and with PCS. The respective normalized heterodyne decay functions, in the case of TDFRS, and the normalized electric field autocorrelation function, measured in a standard homodyne experiment, are plotted in Figure 10. The PCS correlation function has been measured at 90° and rescaled to the q range of the TDFRS experiment, corresponding to approximately 2°. The difference in the average decay time is immediately obvious, with PCS being the slowest and short exposure TDFRS the fastest.

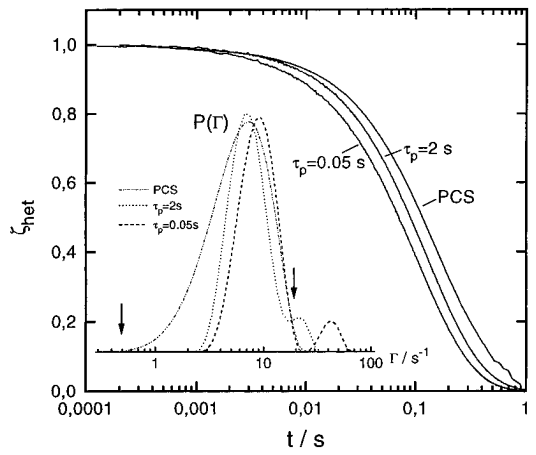

Figure 10. Normalized decay curves from heterodyne short exposure (τ_p = 0.05 s) and long exposure (τ_p = 2 s) TDFRS and electric field autocorrelation function from homodyne PCS for broad PS in ethyl acetate. The corresponding rate distributions have been determined by CONTIN. The arrows mark the inverse exposure times τ_p^{-1}.

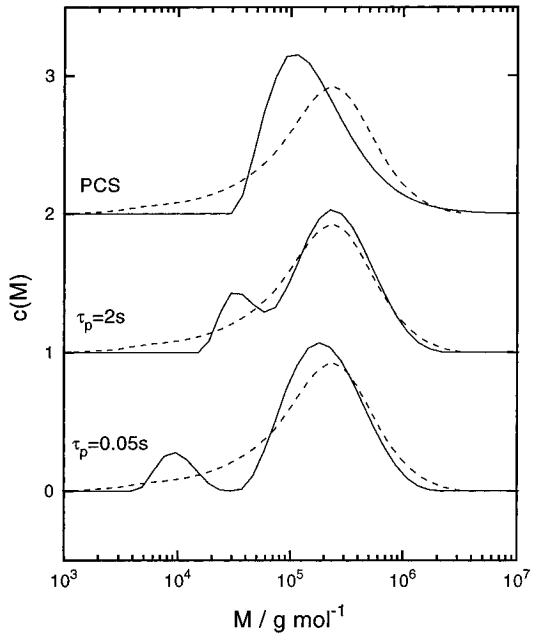

Figure 11. Molar mass distributions computed from the rate distributions in Figure 10. The dashed curves represent the distribution as determined by SEC.

Also shown in Figure 10 are the rate distributions as extracted from the three decay curves.

The 0.05 s exposure does not fully conform to the short exposure criterion $\tau_p \ll \tau_k$. Hence, eq 39, instead of eq 38, must be used for the computation of the molar mass distribution. The normalized molar mass distributions as obtained from the three optical experiments are superimposed to the molar mass distribution obtained from size exclusion chromatography (SEC) in Figure 11.

The general features, a dominant contribution at high molar mass and a long tail at low molar masses, are reasonably reproduced by the two TDFRS measurements, whereas the low molar mass tail is invisible in the PCS distribution. This behavior is mainly caused by the strong overestimation of high molar mass components in the PCS correlation function. TDFRS, especially in the short exposure limit, does not suffer from this severe limitation (eqs 36 and 37). The given molar mass distribution covers approximately 3 orders of magnitude. Hence, even in the long exposure limit,

Table 2. Number Average (M_n), Weight Average (M_w), and *z*-Average (M_z) Molar Masses (in kg mol^{-1}) of a Broad PS As Measured by the Different Techniques[a]

	SEC	TDFRS (0.05 s)	TDFRS (2 s)	PCS
M_n	57	58	107	121
M_w	285	237	275	262
M_z	640	434	509	1229

[a] TDFRS (0.05 s) corresponds approximately to the short, and TDFRS (2 s), to the long exposure limit.

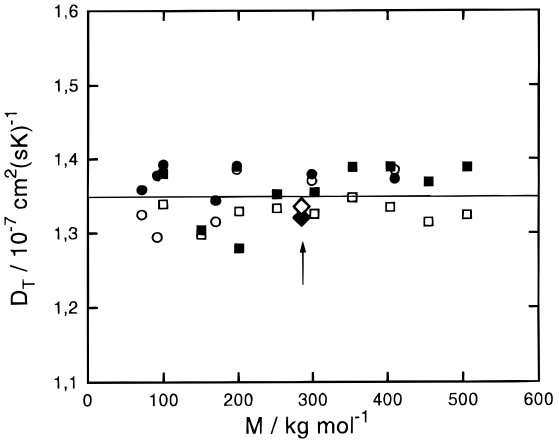

Figure 12. Thermal diffusion coefficient of PS in ethyl acetate as a function of molar mass: (○) nearly monodisperse samples; (□) bimodal mixture of $M_{w,1}$ = 49 kg/mol and $M_{w,2}$ = 556 kg/mol; (◇) polydisperse sample (marked with arrow). The open symbols were obtained from the saturation amplitude; the filled ones, from the initial slope.

the underestimation of the lower end of the distribution in the decay curve is $1000^{-0.516} \approx 0.028$, as compared to 0.001 in PCS. In short exposure TDFRS all molar masses contribute approximately equally.

Obviously, the TDFRS distributions are also not perfect, as can be seen from their bimodal structure. This ambiguity, which is rooted in the problem of obtaining the correct fine structure of a broad rate distribution from an inverse Laplace transform of the corresponding multiexponential decay curve by e.g. CONTIN is certainly a fundamental limitation of the method. By choosing a different regularization parameter a smoother solution with a single peak can be enforced. Without additional a priori knowledge such a choice can, however, hardly be justified. This problem of spurious peaks in a CONTIN analysis is not specific to TDFRS but also known from PCS. Contrary to the fine structure, the lower moments of the distribution are rather insensitive to the choice of the regularization parameter. In Table 2 the number average, the weight average, and the *z*-average molar masses, as obtained from the different distributions functions, are summarized.

Good agreement is found for M_w, less for M_n and M_z, with particularly strong deviations of the PCS results, where the correct determination of M_n is complicated by the long low molar mass tail.

Thermal Diffusion Coefficients. The thermal diffusion coefficient, D_T, can be determined either from the initial slope (eq 27) in an experiment of arbitrary excitation length or from the steady state amplitude and the initial decay (eq 32).

Figure 12 shows D_T for PS in ethyl acetate as a function of molar mass. All measurements were done at a concentration of $c \approx 0.006$, and both methods described above were used for data evaluation, yielding

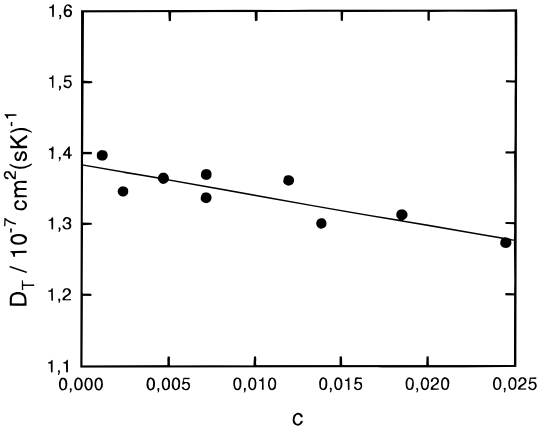

Figure 13. Concentration dependence of D_T for PS in ethyl acetate.

identical results. The circles correspond to nearly monodisperse samples ($M_w/M_n = 1.03-1.05$), the squares to mixtures of $M_1 = 49$ kg mol^{-1} and $M_2 = 556$ kg mol^{-1} of variable composition, which are plotted at the respective weight average molar mass M_w. The diamonds correspond to the polydisperse sample from Figure 11. No molar mass dependence of D_T is observed, in accordance with the literature,[1] and the same results are obtained from monodisperse and polydisperse samples. The average value is $D_T = 1.35 \times 10^{-7}$ cm^2 (s K)$^{-1}$ (T = 24 °C). In the literature $D_T = 1.16 \times 10^{-7}$ cm^2 (s K)$^{-1}$ (T = 22 °C) is reported from TFFF experiments.[1] In a previous but less accurate TDFRS experiment $D_T = 1.25 \times 10^{-7}$ cm^2 (s K)$^{-1}$ was found.[6] The contrast factors $(\partial n/\partial c)_{p,T} = 0.193$ and $(\partial n/\partial T)_{p,c} = -5.14 \times 10^{-4}$ K^{-1} have been measured as described in the Experimental Section.

The concentration dependence of D_T in the dilute regime is only very weak (Figure 13), and the concentration correction can be neglected when comparing the results.

Summary and Conclusion

The treatment of polydispersity effects in TDFRS experiments on dilute polymer solutions has been outlined in theory and supported by experiments on solutions of linear PS in toluene and ethyl acetate and PS microgels in toluene. From a time domain TDFRS experiment various averages of the transport coefficients can be obtained: D_T, $\langle S_T \rangle_c$, $\langle D \rangle_c$, and $\langle D \rangle_{c/D}$. The latter is of particular interest, since it gives access to the weight average hydrodynamic radius $\langle R_h \rangle_c$, a quantity that is difficult to measure otherwise.

The information content of the heterodyne TDFRS decay function shows some similarities to the electric field autocorrelation function in PCS. The signal stems, however, from a coherent excitation of the sample with a well-defined q vector, in contrast to the statistical fluctuations. By employing excitation pulses of variable length the statistical weights of the individual components can be varied between c and cM^b, as compared to the fixed statistical weight cM in PCS, which strongly overestimates high molar mass components.

Using CONTIN the deconvolution of the decay function and the computation of the molar mass distribution has been demonstrated for a bimodal mixture and a broadly distributed PS sample.

For the bimodal mixture a quantitative separation of both components could be achieved. An exact reproduction of the broad molar mass distribution as determined by SEC could neither be achieved by TDFRS nor by PCS. However, a satisfactory agreement between SEC and TDFRS could be found for the averages M_n, M_w, and M_z. Best results are obtained from short exposure TDFRS. The price that has to be paid for the constant statistical weights is a lower signal intensity than in the long exposure experiment. To overcome this limitation, which is caused by the low power density in the excitation spectrum when short exposure pulses are used, stochastic excitation together with correlation techniques will be implemented in the future.

Acknowledgment. The authors thank M. Wintermantel for supplying the PS with the broad molar mass distribution, S. Stölken for the microgels, C. Rosenauer for the PCS measurements, and B. Müller for the measurement of the refractive index increments. W. Köhler is grateful to H. Winter for the discussion of frequency domain TDFRS experiments.

References and Notes

(1) Schimpf, M. E.; Giddings, J. C. *J. Polym. Sci.* **1989**, *B27*, 1317−1332.
(2) Meyerhoff, G.; Nachtigall, K. *J. Polym. Sci.* **1962**, *57*, 227.
(3) Kesner, L. F.; Giddings, J. C.; Caldwell, K. D. In *Determination of Molecular Weight*; Cooper, A. R., Ed.; John Wiley & Sons, Inc.: New York, 1989; Chapter 12.
(4) Kirkland, J. J.; Rementer, S. W.; Yau, W. W. *J. Appl. Polym. Sci.* **1989**, *38*, 1383.
(5) Antonietti, M.; Briel, A.; Tank, C. *Acta Polym.* **1995**, *46*, 254.
(6) Köhler, W. *J. Chem. Phys.* **1993**, *98*, 660.
(7) Köhler, W.; Rossmanith, P. *Int. J. Polym. Anal. Characterization* **1995**, *1*, 49.
(8) Köhler, W.; Rosenauer, C.; Rossmanith, P. *Int. J. Thermophys.* **1995**, *16*, 11.
(9) Köhler, W.; Rossmanith, P. *J. Phys. Chem.* **1995**, *99*, 5838.
(10) Kolodner, P.; Williams, H.; Moe, C. *J. Chem. Phys.* **1988**, *88*, 6512.
(11) Ecenarro, O.; Madariaga, J. A.; Navarro, J.; Santamaria, C. M.; Carrion, J. A.; Saviron, J. M. *J. Phys. Condens. Matter* **1990**, *2*, 2289.
(12) Rossmanith, P., Ph.D. thesis, Johannes Gutenberg-Universität, Mainz, 1995.
(13) Bloisi, F.; Vicari, L.; Cavaliere, P.; Martellucci, S.; Quartieri, J.; Mormile, P.; Pierattini, G. *Appl. Phys.* **1987**, *B44*, 103.
(14) Tyrrell, H. J. V. *Diffusion and heat flow in liquids*; Butterworth: London, 1961.
(15) Bloisi, F. *Opt. Commun.* **1988**, *68*, 87.
(16) Koppel, D. E. *J. Chem. Phys.* **1972**, *57* (11), 4814.
(17) King, T. A.; Treadaway, M. F. *J. Chem. Soc., Faraday Trans.* **1977**, *73*, 1616.
(18) Provencher, S. W. *Comput. Phys. Commun.* **1982**, *27*, 229−242.
(19) Stock, R. S.; Ray, W. H. *J. Polym. Sci., Polym. Phys.* **1985**, *23*, 1393.
(20) Chu, B. *Laser Light Scattering*; Academic Press: New York, 1991.
(21) Corti, M.; Degiorgio, V.; Giglio, M.; Vendramini, A. *Opt. Commun.* **1977**, *23* (2), 282.
(22) Stölken, S.; Bartsch, E.; Sillescu, H.; Lindner, P. *Prog. Colloid Polym. Sci.* **1995**, *98*, 155.
(23) Becker, A.; Köhler, W.; Müller, B. *Ber. Bunsen-Ges. Phys. Chem.* **1995**, *99*, 600.
(24) Schaefer, D. W.; Han, C. C. In *Dynamic light scattering*; Pecora, R., Ed.; Plenum Press: New York, 1985, Chapter 5.

MA9516302